

# Supplementary Material

## Secondary instabilities in Taylor Couette flow of shear thinning fluids

S. TOPAYEV<sup>1</sup>, C. NOUAR<sup>1</sup> and J. DUSEK<sup>2</sup>

<sup>1</sup>LEMETA, UMR 7563, CNRS - Université de Lorraine, 2 Avenue de la Fort de Haye, BP 90161  
54505 Vandoeuvre Lès Nancy, France

<sup>2</sup>ICUBE, UMR 7357, CNRS - Université de Strasbourg, 2 rue Boussingault, 67000 Strasbourg,  
France

(Received 4 November 2021)

### 1. Supplementary section S1: Numerical method

#### 1.1. Weak formulation

The governing equations (2.2) and (2.1) combined with (2.4) and (2.6) are solved numerically using the finite element solver FreeFem++ (Hecht 2012). The weak formulation of equations (2.1,2.2) reads:

$$\int_{\Omega} q \nabla \cdot \mathbf{u} d\Omega = 0, \quad (1.1)$$

$$\int_{\Omega} (\partial_t \mathbf{u} + (\mathbf{u} \cdot \nabla) \mathbf{u}) \cdot \mathbf{v} d\Omega = \int_{\Omega} (p \nabla \cdot \mathbf{v} - \boldsymbol{\tau} : \nabla \mathbf{v}) d\Omega \quad (1.2)$$

$$+ \int_{\partial\Omega} \mathbf{v} \cdot (-p \mathbf{I} + \boldsymbol{\tau}) \cdot \mathbf{n} d\partial\Omega.$$

where  $\Omega$  is the volume occupied by the fluid and  $\partial\Omega$  is its boundary. Given the axisymmetry of the problem, cylindrical coordinates are used and the integration over  $\theta$  yields the factor  $2\pi$  so that  $d\Omega = 2\pi r dr dz$  and  $d\partial\Omega = 2\pi r dl$ , where  $dl$  is the length of an elementary segment of the 2D boundary  $\partial\mathcal{D}$  in the axial-radial plane. In what follows, the

common factor  $2\pi$  will be left out and a 2D formulation is obtained. In this formulation,  $\mathbf{n}$  is the unit vector normal to the boundaries, pointing outward of the rectangle  $\mathcal{D}$ . The test functions  $q$  and  $\mathbf{v}$  are associated to the pressure  $p$  and the velocity  $\mathbf{u}$ , respectively.  $\mathbf{I}$  stands for the identity tensor. The surface term is zero for all the three types of boundary conditions specified in the previous section.

### 1.2. Time and space discretization

Discretizing the time derivative term by a first order backward Euler scheme and treating the nonlinear inertial terms and the nonlinear viscosity explicitly (Jenny *et al.* 2015), we get

$$\int_{\mathcal{D}} q \nabla \cdot \mathbf{u}_{n+1} r dr dz = 0, \quad (1.3)$$

$$\int_{\mathcal{D}} \left[ \frac{\mathbf{u}_{n+1}}{\Delta t} \cdot \mathbf{v} - p_{n+1} \nabla \cdot \mathbf{v} + \mu(\mathbf{u}_n) \dot{\gamma}(\mathbf{u}_{n+1}) : \nabla \mathbf{v} \right] r dr dz = \int_{\mathcal{D}} \left[ \left( \frac{\mathbf{u}_n}{\Delta t} - (\mathbf{u}_n \cdot \nabla) \mathbf{u}_n \right) \cdot \mathbf{v} \right] r dr dz. \quad (1.4)$$

For the space discretization of equations (1.3) and (1.4), a triangular mesh with  $40 \times 40L$  identical rectangles in the domain  $\mathcal{D}$ , each of them is divided into two triangles of equal area is used. A convergence test has also been performed with  $60 \times 60L$  rectangles. The finite element spaces used to discretize the velocity and the pressure are the Inf-Sup stable Taylor-Hood finite elements P2P1, i.e. quadratic continuous functions for velocity trial and test functions and piecewise continuous linear functions for pressure trial and test functions. The resulting algebraic system is solved with an iterative Uzawa Conjugate Gradient algorithm with a Cahouet-Chabart preconditionner (Hecht 2012; Cahouet & Chabard 1988). The matrix inversions are performed with the UMFPack solver embedded in FreeFem++. During the transient stages, the time step must satisfy the CFL condition to insure the accuracy and the numerical stability. In our simulations, the time step  $\Delta t$

always verifies  $\Delta t \leq \frac{h}{u_{max}}$ , where  $h$  is the smallest equivalent diameter of mesh elements and  $u_{max}$  is the maximum value of the norm of  $\mathbf{u}$ .

Concerning the initial conditions, the flow field at  $t = 0$  is given by specifying the initial values of the velocity components in the entire domain. We have used the Couette flow solution of a Carreau fluid between infinite cylinders as initial conditions at a Reynolds number below the critical value. This Couette flow solution determined numerically has been first regularized to take into account the singularity in the azimuthal velocity at the lower surface. A continuation method is then used where each new simulation is started with the permanent regime solution corresponding to the closest set of parameters as initial condition.

In the case of axial periodic boundary conditions, the initial condition is a velocity field which corresponds to divergence-free rolls:

$$\mathbf{u}'(r, z, t = 0) = A_0 (u'_r \mathbf{e}_r + u'_z \mathbf{e}_z), \quad (1.5)$$

where  $A_0$  is the initial amplitude of the perturbation, and

$$u'_r = \cos(kz) (r - r_1)^2 (r - r_2)^2, \quad (1.6)$$

$$u'_z = -\sin(kz) (r - r_1) (r - r_2) \frac{4r - 2(r_1 + r_2) + \frac{(r-r_1)(r-r_2)}{r}}{k}. \quad (1.7)$$

The shear-thinning behavior of the Carreau model (2.6) depends on the shear-thinning index  $n_c$  and the dimensionless constant time  $\lambda$ . Shear-thinning effects increase either by increasing  $\lambda$  or by decreasing  $n_c$ . Here, we have fixed  $\lambda = 200$  and the numerical results are presented for  $n_c = 0.5$  and  $n_c = 0.2$ . For  $n_c = 0.5$ , Taylor vortices fill all the annular space, whereas for  $n_c = 0.2$ , Taylor vortices are strongly squeezed against the inner wall. One can also recall that when  $\lambda \geq 30$ , this parameter has practically no effect on the base flow as well as on the size of vortices (Alibenyahia *et al.* 2012; Topayev *et al.* 2019).

## 2. Supplementary section S2: Validation of the numerical method

### 2.1. Comparison with linear theory

Taylor-Couette configuration with periodic boundary conditions is used as a model to approximate infinite cylinders. To determine the threshold of the primary bifurcation, we compute the transient evolution of the velocity, starting with initial conditions (1.5)-(1.7), with a very small amplitude  $A_0 = 10^{-6}$ . For a Newtonian fluid and a radius ratio  $\eta = 0.4$ , we compute the time evolution of the flow at  $Re = 68.08$  and  $Re = 68.5$ , i.e. around the value of the critical Reynolds number  $Re_c = 68.296542$  (Alibenyahia *et al.* 2012; Topayev *et al.* 2019). From exponential fits of the time series, we extract the linear growth rates  $\sigma(Re = 68.08) = -0.086391$  and  $\sigma(Re = 68.5) = 0.081148$ . A linear fit between these values provides a critical value  $Re_c = 68.2972$  very close to that given in the literature.

A similar result was obtained for a shear-thinning fluid. For instance, for a Carreau fluid with  $n_c = 0.5$ ,  $\lambda = 100$  and  $\eta = 0.4$ , the linear stability analysis (Alibenyahia *et al.* 2012; Topayev *et al.* 2019) gives  $Re_c = 3.5770645$ . Using the same initial condition as previously, linear growth-rates are computed using the method of Sec. 1 at two Reynolds numbers around  $Re_c$ . After exponential fits, we obtain  $\sigma(Re = 3.5663) = -0.0075602$  and  $\sigma(Re = 3.5871) = 0.0064292$ . A linear fit between these two values leads to a critical Reynolds number of  $Re_c = 3.5775708$  very close to that given predicted by the linear theory for infinite cylinders (Topayev *et al.* 2019).

### 2.2. Comparison with weakly nonlinear theory

In table T1 the torque obtained using the method of Sec. 1 for a Newtonian fluid at  $\eta = 0.5$  is compared with the weakly nonlinear stability calculations of Davey (1962) and those of Topayev *et al.* (2019). Here the torque  $T$  has been non-dimensionalized by

Re	Torque	Torque, theoretical	Torque, theoretical	Torque
Reynolds number	Sec. 1 method	(Topayev <i>et al.</i> 2019)	(Davey 1962)	(Fasel & Booz 1984)
70.0	17.1594	17.1572	17.1544	17.1537
75.0	18.1741	18.2090	18.1089	18.1627
80.0	19.0700	19.1164	18.6183	19.0527
85.0	19.8707	19.8909	19.5375	19.8490
90.0	20.5954	20.5543	20.0800	20.5692
95.0	21.2567	21.1265	20.5391	21.2267

Supplementary Table T1: Newtonian fluid with  $\eta = 0.5$ . Variation of the torque at the inner cylinder as a function of Reynolds number. Comparison with weakly nonlinear stability results of Topayev *et al.* (2019) as well as with the numerical results of Fasel & Booz (1984).

the reference torque  $T_{ref} = \mu R_1^2 \Omega_1 \ell$  where  $\ell$  is the length of the cylinders. In the low supercritical regime the agreement with both Davey's and Topayev *et al.*'s data is very good. Nevertheless, one can note that our numerical solutions are closer to Topayev *et al.*'s results than to Davey's ones. This is not surprising since Davey's analysis is based on expansion at cubic order about the critical Reynolds number, whereas in Topayev *et al.* (2019), the expansion is pushed until seventh order.

Comparison with weakly nonlinear theory in the case of a shear-thinning fluid is displayed in table T2. A Carreau fluid with  $n_c = 0.5$  and  $\lambda = 100$  is considered. The radius ratio is  $\eta = 0.4$ . As it can be observed, our numerical solutions are in very good agreement with Topayev *et al.*'s results.

Re	Torque	Torque, theoretical
Reynolds number	method of Sec. 1	(Topayev <i>et al.</i> 2019)
3.5810	0.54993	0.54975
3.9348	0.56953	0.56572
4.2925	0.58656	0.580353
4.6502	0.59795	0.59242

Supplementary Table T2: Carreau fluid with  $n_c = 0.5$ ,  $\lambda = 100$  and  $\eta = 0.4$ . Variation of the torque at the inner cylinder on Reynolds number. Comparison with weakly nonlinear stability results of Topayev *et al.* (2019)

### 2.3. Comparison with literature in strongly nonlinear regime

To validate the numerical tool described in Sec. 1, in a strongly nonlinear regime, our numerical results are compared with those obtained by Fasel & Booz (1984) for a Newtonian fluid at  $\eta = 0.5$ . In their numerical study, the computations were carried out under the assumption of axisymmetric flow structure, with  $L = 2$  and periodic boundary conditions at both ends of cylinders. Note that  $L = 2$  is very close to the axial wavelength at critical conditions  $\Lambda = 1.9858$ . Our numerical solutions obtained using a single wavelength fluid column with periodic boundary conditions presented in table T5 at different Reynolds numbers show excellent agreement with the DNS study of Fasel & Booz (1984). Additional computations done with two wavelengths fluid column gives the same results.

## 3. Supplementary section S3: Experimental protocol

To observe flow structures corresponding to various Re in the Taylor-Couette geometry, the Reynolds number is slowly increased with time starting from a stationary inner

cylinder. Actually, we have first evaluated the critical Reynolds number,  $Re_c$ , for the onset of Taylor vortices from the linear theory. The velocity of rotation of the inner cylinder is increased from  $Re = 0$  to  $Re = 0.8 Re_c$  in one hour. In this first step, the ramping rate agrees with the criterion of Dutcher & Muller (2009): the nondimensional acceleration rate  $dRe/dt_d$ , where  $t_d$  is the time dimensionalized with the viscous diffusion time scale  $\rho d^2/\mu$ , should be less than unity to ensure that the flow can be considered to be quasisteady. The values of  $dRe/dt_d$  and  $d\Omega_1/d\hat{t}$  are listed in Table T3, with  $\hat{t}$  the dimensional time. In the second step, i.e. from  $Re = 0.8 Re_c$ ,  $\Omega_1$  was increased in small steps of  $\Delta\Omega_1$  with waiting times sufficiently long to assure static conditions. Typical values of  $\Delta\Omega_1$  is 0.21 rad/s. However, near criticality, the increment  $\Delta\Omega_1$  was reduced to 0.105 rad/s. Above the onset of TVF, the step  $\Delta\Omega_1$  and the waiting time period were adapted to have a balance between the need to avoid unsteady effects and the requirements that the measurements were performed over a reasonable time. Experiments typically lasted approximately 6 to 10 hours. Temperature measurements of the working fluid before and after an experiment indicated that the temperature change was less than 1°C.

#### 4. Supplementary section S4: Influence of the endwalls: Numerical results

The objective of this section is to check if the endwall boundary conditions have an effect on the onset of Taylor vortices in the case of purely viscous shear-thinning fluid for a quite small aspect ratio  $L = 10$ .

For a purely viscous fluid, at  $Re \ll Re_c$  and far from the endwalls, the stable flow is geostrophic. The fluid is in equilibrium under the centrifugal force and the pressure gradient. Close to the stationary bottom endwall, the no-slip boundary condition results

---

#	Concentration	$d\Omega_1/d\hat{t}$ (rad/s <sup>2</sup> )	dRe/dt <sub>d</sub>
(1)	glycerol aqueous solution	0.872e-3	1.006e-2
(2)	1000 ppm	0.909e-3	1.97e-2
(3)	2000 ppm	0.691e-3	2.01e-4
(4)	3000 ppm	2.035e-3	1.51e-6

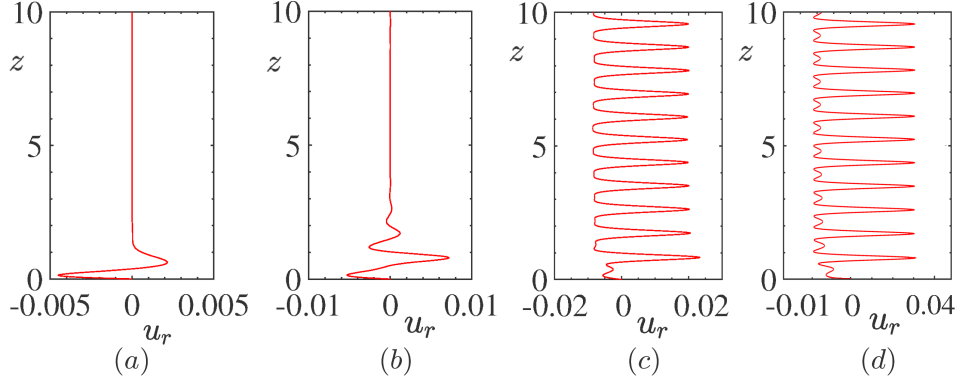
---

Supplementary Table T3: Experimental conditions used in the various experiments: acceleration rate during the phase where the velocity of the inner cylinder is increased from 0 to  $0.8 \text{ Re}_c$ .

in an azimuthal velocity lower than that far from the endwall. The imbalance between the pressure gradient force and the centrifugal force near the bottom endwall, results in a force that drives the fluid radially inwards (Czarny *et al.* 2003). This radial inflow induces an axial downward flow near the outer cylinder and an axial upward flow near the inner one, yielding a vortex situated at the bottom wall. As the Reynolds number is increased more counter rotating vortices appear. Below  $\text{Re}_c$ , the strength of the vortices decays exponentially (Ahlers *et al.* 1986; Lücke *et al.* 1985; Pfister & Rehberg 1981). However, the exponential decay length diverges as  $|\epsilon|^{-1/2}$ . Hence, a finite system of length  $L$  will be completely filled with detectable vortices for  $\epsilon \geq -L^{-2}$  (Ahlers *et al.* 1986). These counter-rotating vortices appear quite similar to Taylor vortices and have almost the same axial extent (Czarny *et al.* 2003). Numerical simulations done with  $L = 10$ , for a Carreau fluid of rheological parameters  $n_c = 0.2$  and  $\lambda = 200$  show that around the middle of the annular domain and at  $\epsilon \leq -0.01$ , the vortices induced by the endwalls boundary conditions are very weak. This is clearly shown by figure F1 where we have represented

the radial velocity profile along the axial line,  $r = 0.8$ , passing through the center of vortices (position of minimum speed in the radial plane,  $\sqrt{u_r^2 + u_z^2}$ ). At  $\epsilon = -0.01$ , the maximum radial velocity is about 0.7% of the surface speed of the inner cylinder reached near the bottom endwall. When  $\epsilon > 0$ , vortices due to centrifugal instability are observed and their strength increases with increasing Reynolds number. Around the middle of the height of the annular space ( $z = 5$ ), we have found a wavenumber  $k^{num} = 8.39$  which is in very good agreement with the theoretical value  $k_c = 8.4055$  (Topayev *et al.* 2019). Therefore, there is practically no effect of endwalls boundary conditions on the onset of TVF even for a quite small aspect ratio  $L = 10$ . At the middle of the height of the annular space, the periodicity of the cells is well described by the linear theory.

Note that in the TVF regime the maximum outflow (positive) velocity is larger than the maximum inflow (negative) velocity. For instance, at  $\epsilon = 0.06$ , the ratio between the maximum outflow and the maximum inflow is  $\approx 3.6$  and the width of the inflow region is 2.4 times that of the outflow region as measured between zero-crossings.



Supplementary Figure F1: Carreau fluid with  $n_c = 0.2$  and  $\lambda = 200$ . Radial velocity component along the axial line,  $r = 0.8$ , passing through the center of vortices. **(a)**  $\epsilon = -0.1$ , **(b)**  $\epsilon = -0.01$ , **(c)**  $\epsilon = 0.03$  and **(d)**  $\epsilon = 0.06$ . For  $n_c = 0.2$ ,  $\lambda = 200$ , the linear theory assuming infinite cylinders gives  $\text{Re}_c = 1.1643$  (Topayev *et al.* 2019).

#	Concentration	$n_c$	$\mu_0(\text{Pa}\cdot\text{s})$	$\lambda_f(\text{s})$	$\lambda$
(1)	glycerol aqueous solution	1	0.088	-	-
(2)	850 ppm	0.52	0.13	2.78	0.40
(3)	1000 ppm	0.5	0.33	8.48	3.14
(4)	1200 ppm	0.45	1.64	18.93	34.5
(5)	1500 ppm	0.41	3.38	26.51	99.6
(6)	2000 ppm	0.34	5.85	30.36	197.4
(7)	3000 ppm	0.23	27.48	47.66	1455.2

Supplementary Table T4: The main rheological parameters of aqueous xanthan gum solution: shear-thinning index  $n_c$ , zero shear viscosity  $\mu_0$  and characteristic time of the fluid  $\lambda_f$ , at different concentrations.

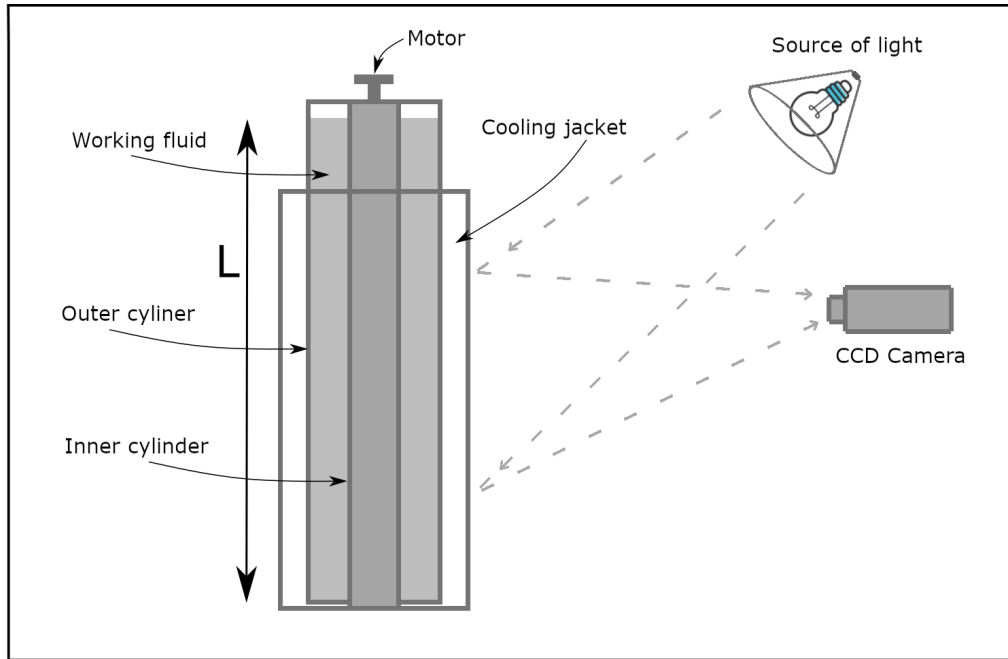
Re	Torque	Torque
Reynolds number	method of Sec. 1	(Fasel & Booz 1984)
100	21.8653	21.8352
125	24.3584	24.3199
150	26.3074	26.2646
175	27.9669	27.9276
200	29.4749	29.4266

Supplementary Table T5: Newtonian fluid with  $\eta = 0.5$ . Variation of the torque at the inner cylinder on Reynolds number. Comparison with numerical results of Fasel & Booz (1984)

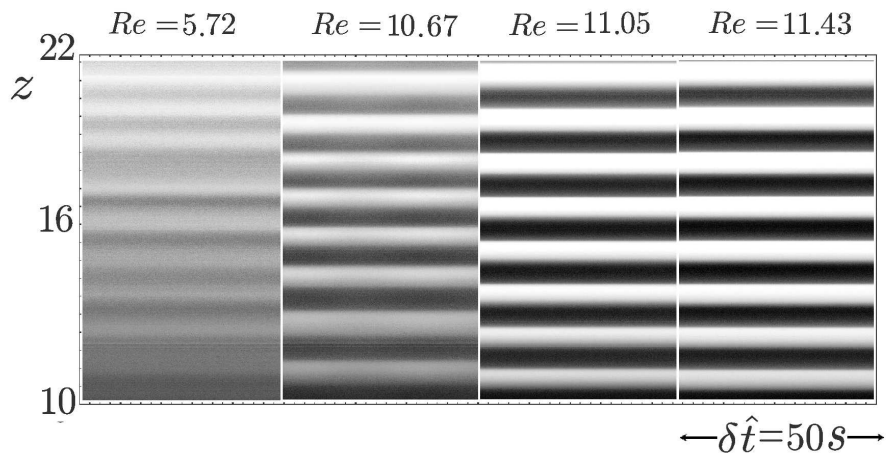
---

#	Concentration	$n_c$	$Re_c$	$Re_c^{exp}$	$k_c$	$k_c^{finite}$	$k_c^{exp}$
(1)	0 ppm	1	68.296	68.74	3.1834	3.24	3.27
(2)	1000 ppm	0.5	11.106	11.05	3.5235	3.63	3.72
(3)	2000 ppm	0.344	1.6944	1.69	4.5159	4.42	4.37
(4)	3000 ppm	0.23	0.5179	0.512	6.8418	6.77	6.55

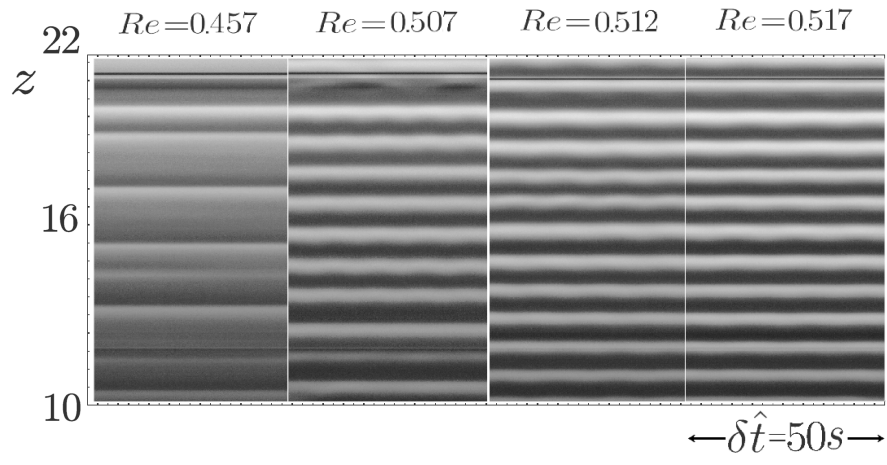
Supplementary Table T6: Comparison between theoretical and experimental critical conditions for Newtonian and aqueous solution of xanthan gum at different concentrations



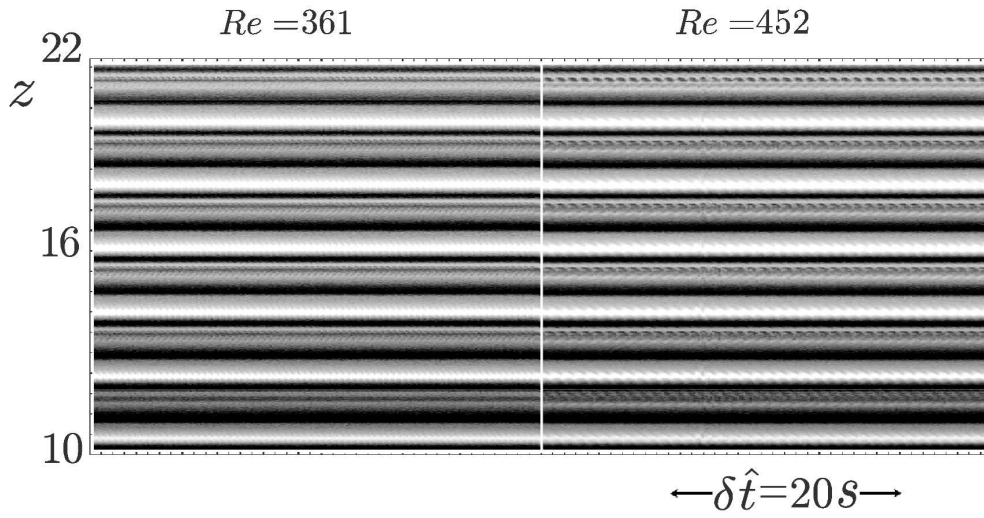
Supplementary Figure F2: Schematic of the experimental set up.



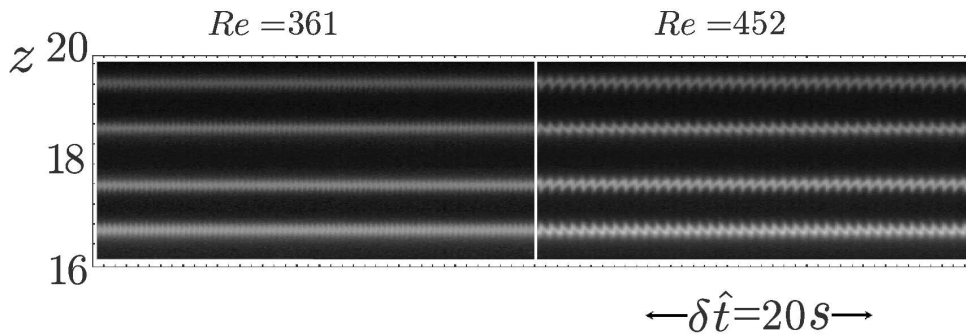
Supplementary Figure F3: Space-time diagrams for aqueous solution of xanthan gum at 1000 ppm for  $Re = 5.72, 10.67, 11.05$  and  $11.43$ . The rheological parameters are  $n_c = 0.5$ ,  $\lambda = 3.1$ . For these parameters, the linear theory assuming infinite cylinders gives  $Re_c = 11.1064$  (Topayev *et al.* 2019).



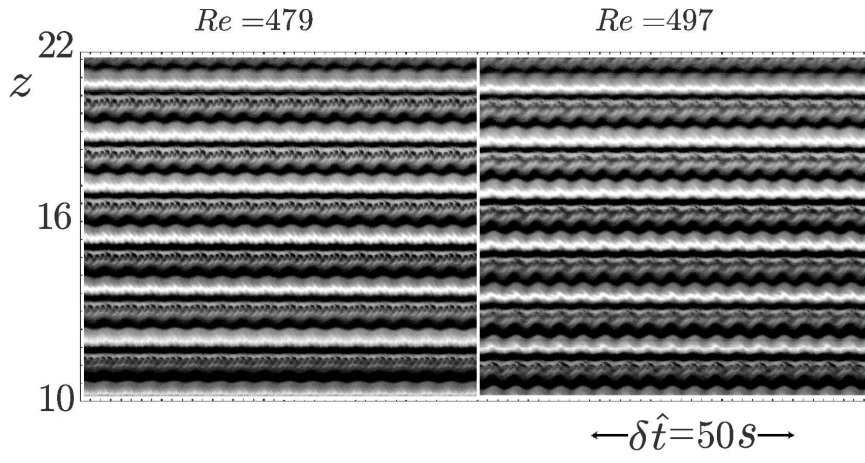
Supplementary Figure F4: Space-time diagrams of xanthan gum 3000ppm at  $Re = 0.457, 0.507, 0.512$  and  $0.517$ . The rheological parameters are  $n_c = 0.23$  and  $\lambda = 1455$ . For this case, the linear theory gives  $Re_c = 0.5180$ .



Supplementary Figure F5: Aqueous glycerol solution. Spatio-temporal diagram in the WVF 1 regime at two Reynolds numbers  $Re = 361$  and  $452$  in the case of WVF 1 regime. The black parallel lines are inflow and outflow boundaries. The vortices are situated between these lines. Adjacent to each vortex is another vortex that circulates in the opposite sense. Neighboring vortices appear darker or lighter. Below each bright vortex there is an outflow boundary and above each bright vortex an inflow boundary.



Supplementary Figure F6: Aqueous glycerol solution. Visualization of the cross-section of the flow in the  $r - z$  plane. Spatio-temporal diagrams in the WVF 1 regime at  $Re = 361$  and  $452$ .



Supplementary Figure F7: Aqueous glycerol solution. Spatio-temporal diagram in WVF II at  $Re = 479$  and  $497$ .

## REFERENCES

- AHLERS, G., CANNELL, D.S., DOMINGUEZ-LERMA, M.A. & HEINRICHS, R. 1986 Wavenumber selection and Eckhaus instability in Couette-Taylor flow. *Physica D: Nonlinear Phenomena* **23** (1-3), 202–219.
- ALIBENYAHIA, B., LEMATRE, C., NOUAR, C. & AIT-MESSAOUDENE, N. 2012 Revisiting the stability of circular Couette flow of shear-thinning fluids. *J. Non-Newtonian Fluid Mech.* **183**, 37–51.
- CAHOUET, J & CHABARD, J-P 1988 Some fast 3d finite element solvers for the generalized stokes problem. *Int. J. Numer. Methods Fluids* **8** (8), 869–895.
- CZARNY, O., SERRE, E., BONTOUX, P. & LUEPTOW, R.M. 2003 Interaction between Ekman pumping and the centrifugal instability in Taylor–Couette flow. *Phys. Fluids* **15** (2), 467–477.
- DAVEY, A. 1962 The growth of Taylor vortices in flow between rotating cylinders. *J. Fluid Mech.* **14** (3), 336–368.
- DUTCHER, CARI S & MULLER, SUSAN J 2009 Spatio-temporal mode dynamics and higher order transitions in high aspect ratio newtonian Taylor-Couette flows. *J. Fluid Mech.* **641**, 85.
- FASEL, H & BOOZ, O 1984 Numerical investigation of supercritical Taylor-vortex flow for a wide gap. *J. Fluid Mech.* **138**, 21–52.
- HECHT, FRÉDÉRIC 2012 New development in freefem++. *Journal of numerical mathematics* **20** (3-4), 251–266.
- JENNY, M., PLAUT, E. & BRIARD, A. 2015 Numerical study of subcritical Rayleigh–Bénard convection rolls in strongly shear-thinning Carreau fluids. *J. Non-Newtonian Fluid Mech.* **219**, 19–34.
- LÜCKE, M, MIHELICIC, M & WINGERATH, K 1985 Front propagation and pattern formation of Taylor vortices growing into unstable circular couette flow. *Phys. Rev. A* **31** (1), 396.
- PFISTER, G & REHBERG, I 1981 Space-dependent order parameter in circular Couette flow transitions. *Phys. Lett. A* **83** (1), 19–22.
- TOPAYEV, S., NOUAR, C., BERNARDIN, D., NEVEU, A. & BAHRANI, S.A. 2019 Taylor-vortex flow in shear-thinning fluids. *Phys. Rev. E* **100** (2), 023117.